Separation and Purification Technology 342 (2024) 127042

Contents lists available at ScienceDirect

Separation and Purification Technology

journal homepage: www.elsevier.com/locate/seppur

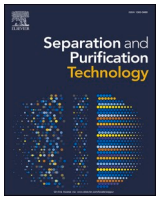

Green photocatalytic mixed matrix membranes for simultaneous arsenic photo-oxidation and water recovery via membrane distillation

Sergio Santoro [a], Jessica Occhiuzzi [b], Marco Aquino [a], Antonio Politano [b], Salvatore Straface [a], Giuseppe D'Andrea [a], Cristobal Carrillo [c,d], Reyes Mallada [c,d], Andreina Garcia [e,f], Humberto Estay [f], Dimitrios Xevgenos [g], Pietro Argurio [a], Efrem Curcio [a,*]

[a] Department of Environmental Engineering, DIAm, University of Calabria, Via Pietro Bucci CUBO 44/A, 87036 Rende, CS, Italy
[b] Department of Physical and Chemical Sciences, University of L'Aquila, 67100 L'Aquila, Italy
[c] Instituto de Nanociencia y Materiales de Aragon (INMA), CSIC-Universidad de Zaragoza, C/Poeta Mariano Esquillor, s/n, 50018 Zaragoza, Spain
[d] Department of Chemical Engineering and Environmental Technologies, Universidad de Zaragoza, C/Poeta Mariano Esquillor, s/n, 50018 Zaragoza, Spain
[e] Mining Engineering Department, FCFM, Universidad de Chile, Av. Tupper 2069, 8370451 Santiago, Chile
[f] Advanced Mining Technology Center (AMTC), University of Chile, Av. Tupper 2007 (AMTC Building), Santiago, Chile
[g] Engineering Systems & Services Department, Technology Policy & Management Faculty, Delft University of Technology, Jaffalaan 5, 2628 BX Delft, the Netherlands

ARTICLE INFO

Editor: B. Van der Bruggen

Keywords:
Arsenic
Green Solvent
Membrane Distillation
Photocatalytic Membranes
Photo-oxidation

ABSTRACT

This work proposes an innovative integration of Membrane Distillation (MD) and photo-oxidation for a continuous recovery of water from arsenic (As) contaminated solutions coupled with the oxidation of arsenite (As (III)) into arsenate (As(V)). Polyvinylidene fluoride (PVDF) mixed matrix membranes (MMMs) containing titanium dioxide nanoparticles (TiO_2 NPs) as photocatalyst were developed. A systematic study elucidated the effect of TiO_2 NPs on membranes' morphology prepared via non-solvent-induced phase separation (NIPS) using triethyl phosphate (TEP) as a green solvent for PVDF solubilization. Vacuum membrane distillation (VMD) tests carried out by irradiating the MMMs with ultraviolet (UV) radiation demonstrated the possibility of recovering up to 80 % of the water from As-contaminated synthetic and real multi-ions aqueous solutions from Sila Massif (Italy). The distillate was recovered at a rate of 6.9–7.2 $kg \cdot m^{-2} \cdot h^{-1}$ (feed inlet temperature of 60 °C), while the presence of 7 wt% of TiO_2 in PVDF membranes enabled the photo-oxidation of 95 % of the As(III) to As(V) at a first order kinetic constant of 0.0106 min^{-1}. After 5 cycles of As-remediation experiments, *post-hoc* mechanical testing on the membrane suggested the emergence of polymer embrittlement induced by UV radiation (total irradiation time of 7.5 h), highlighting the urgent need for developing photocatalytic membranes with long-term stability.

Overall, this study elucidates at laboratory scale the performance of a coupled and continuous Membrane Distillation (MD) and photo-oxidation system for arsenic (As) remediation, employing microporous hydrophobic green membranes doped with a photocatalyst.

1. Introduction

Arsenic (As) is a toxic and carcinogenic metalloid [1] and the World Health Organization (WHO) fixed at 10 $\mu g \cdot L^{-1}$ its threshold concentration in drinking-water [2]. The presence of As in the earth's crust [3,4] and its high mobility in aquifers [5] have been for centuries the major causes of As contamination of waterbodies, recently exacerbated by anthropic activities [6–8]. Currently, the global pattern has revealed an alarming presence of As in freshwater in at least seven countries, and more than 100 million people are daily exposed to As-contaminated water [9].

A wide variety of technologies have been explored for As remediation to attain the stringent threshold fixed by the WHO, including coagulation–flocculation, adsorption, ion exchange, and oxidation [10]. The abovementioned strategies are characterized by numerous critical issues such as expensive, time-demanding, and elaborate pre-treatment steps, chemical regeneration stages for adsorbent materials or ion exchange reactions, and the formation of byproducts such as hazardous sludge in coagulation and flocculation processes [10–12].

Moreover, these techniques effectively remove arsenate (H_3AsO_4, As

* Corresponding author.
E-mail address: efrem.curcio@unical.it (E. Curcio).

https://doi.org/10.1016/j.seppur.2024.127042
Received 12 December 2023; Received in revised form 5 March 2024; Accepted 6 March 2024
Available online 7 March 2024

(V)) being dissociated in mild conditions; while they fail in the remediation of arsenite (H_3AsO_3, As (III)), characterized by higher toxicity and mobility, because uncharged for pH below than 9.2 [13]. In fact, zero-valent iron is the most studied As-absorbent material showing an absorption capacity of 36.9 $mg{\cdot}g^{-1}$ for As(V) reduced to 14.3 $mg{\cdot}g^{-1}$ for As(III) [14]. Also popular coagulation-agents such as ferric chloride and chitosan decrease their efficiency in the removal of As(III) in comparison to As(V) from 90 % to 60 % and from 100 % to 80 % respectively [15].

Definitively, the oxidation of As(III) into As(V) is a crucial step before downstream processing. Accordingly, titanium dioxide (TiO_2) has been extensively recognized as an effective photocatalyst for the oxidation of As(III) to As(V) because of the strong oxidation potential of the photogenerated valence band (VB) holes generated upon the absorption of ultraviolet (UV) radiation [13,16].

In recent years, membrane processes have gained increasing success because of their efficiency, inherent modularity, operational simplicity, small footprint, reliability, and environmental friendliness [17–19]. Therefore, membrane technologies are suitable for different approaches aimed at energy-saving and efficient water treatments [20–22], including metal remediation [23,24]. On the basis of the size exclusion mechanism, pressure-driven membrane processes, especially Reverse Osmosis (pore size < 0.5 nm) and Nanofiltration (0.5 nm < pore size < 2 nm), present the tremendous advantage to ensure high As rejection rates independently form the oxidation state [25]. Likewise, the membrane distillation (MD) provides the opportunity to produce high-quality freshwater under a moderate temperature gradient by microporous hydrophobic membranes, enabling the diffusional transport of volatile compounds in the vapor phase into the pores and the theoretical 100 % rejection of non-volatile components [26,27]. In contrast to pressure-driven operations, MD is not limited by osmotic pressure and concentration polarization, thus achieving a high water recovery factor from aqueous solutions (such as up to 90 % from seawater) [28,29]. Other strengths of MD, useful in the remediation of As-contaminated waterbodies, are the negligible impact of feed composition (including the As concentration), presence of other solutes, and pH on the performance of the process [30–32]. Accordingly, different studies have demonstrated the potential of MD operations in the remediation of As-contaminated aqueous solutions, showing rejection rates in the range of 95–100 % [33]. Moreover, recent works have highlighted the prospects of hybridization with renewable energies or waste heat [30] or the exploitation of photothermal nanomaterials [34,35] to sustainably harvest the heat required to vaporize water. In addition, the protraction of MD operation up to a high recovery factor enables the generation of minimal volumes of highly concentrated retentate suitable for a post-treatment process [36].

In our previous work, we demonstrated the effectiveness of MD in recovering up to 98.8 % of high-quality distilled water from As-contaminated solution, while the 83-fold concentrated retentate was subjected to a batch treatment of photocatalysis to convert As(III) to As (V) easily removed by polymer-enhanced ultrafiltration (PEUF) [37].

In the present study, the photocatalyst was directly embodied into hydrophobic microporous membranes prepared according to green routes with the aim to couple for the first time photocatalytic arsenic oxidation technology and membrane distillation together implementing the pioneering concept of photocatalytic MD (PC-MD) for a simultaneous arsenic photo-oxidation and water recovery in the logic of process intensification.

The photocatalytic mixed matrix membranes (MMMs) were prepared via non-solvent-induced phase separation (NIPS) upon the solubilization of polyvinylidene fluoride (PVDF) in a dispersion of TiO_2 in triethyl phosphate (TEP), a green solvent. We systematically elucidated the effects of (i) the influence of the embodiment of the TiO_2 on the physicochemical properties of the photocatalytic membranes, (ii) the feed temperature on the MD performance, and (iii) the TiO_2 loading on the photo-oxidation rate of As(III) to As(V), subsequently removed by an aluminosilicate adsorbent. To assess the feasibility of the process in treating real groundwater, experiments were also conducted using a multi-ion solution contaminated by As(III).

Overall, this work opens new perspectives in implementing an integrated approach that can synergistically combine MD and photocatalytic membrane technologies for continuous As remediation of waterbodies.

2. Materials and methods

2.1. Materials

Polyvinylidene fluoride Grade Solef® 6010 (PVDF, M_w = 322 $kg{\cdot}mol^{-1}$) was supplied by Solvay Specialty Polymers (Italy). Triethyl phosphate (TEP) from Sigma-Aldrich (Italy) was used as the solvent without further purification. Polyvinylpyrrolidone (PVP K17, BASF, Ludwigshafen, Germany, M_w = 9 $kg{\cdot}mol^{-1}$) and polyethylene glycol (PEG, Sigma Aldrich, Milan, Italy, Mw = 200 $g{\cdot}mol^{-1}$) were selected as pore-former agents. TiO_2 nanoparticles (NPs) type P25 purchased from Evonic-Degussa (Germany) with a size of 20 nm, a specific surface area of 44 $m^2{\cdot}g^{-1}$, a band gap of 3.2 eV and containing anatase and rutile phases in a ratio of 4:1 was used as photocatalyst [38].

Sodium metaarsenite $NaAsO_2$ (M_w = 129.91 $g{\cdot}mol^{-1}$, purity of ≥ 98 %) and sodium arsenate dibasic hepta-hydrate $Na_2HAsO_4{\cdot}7H_2O$ (M_w = 312.01 $g{\cdot}mol^{-1}$, purity of ≥ 98 %), both purchased from Sigma-Aldrich (Italy), were used as As(III) and As(V) based salts and solubilized in ultrapure Milli-Q water for the preparation of artificial As-contaminated solution. As(III) (0.06 $mg{\cdot}L^{-1}$) was solubilized into a real water sample from Calabria (Italy) to mimic the As contamination recently observed in the groundwater of Sila Massif (Calabria, Italy) [39].

2.2. Analytical methods

The As concentration was determined by high-resolution continuum source atomic absorption spectrometry (HR-CS AAS). As(III) and As(V) concentrations were quantified by analytical kits MQuant (Merck, Italy) operating in the ranges 0.005–0.5 $mg{\cdot}L^{-1}$ and 0.02–3.0 $mg{\cdot}L^{-1}$ obtaining comparable values with respect to HR-CS AAS measurements (difference < 4 %). Cartridges containing 0.8 g of aluminosilicate purchased from Metalsoft Center (USA) were employed as speciation media able to selectively adsorb As(V)[40].

The ionic composition of real water samples was determined by ion chromatography (Metrohm 861 Advanced Compact IC, Switzerland) using 3.2 mM Na_2CO_3 + 1 mM $NaHCO_3$ solution as the eluent for the anion column Metrosep A Supp 5–250/4.0 and 2 mM nitric acid + 0.25 mM oxalic acid solution for the cation column Metrosep C4–250/4.0.

2.3. Membrane preparation

The polymeric solution was prepared by dissolving 15 wt% of PVDF in TEP at a temperature of 100 °C under magnetic stirring (100 rpm for 8 h); moreover, 5 wt% of PVP and 20 % of PEG were added to the polymeric solution as pore-forming agents.

For the preparation of the photocatalytic MMMs, TiO_2 NPs were previously dispersed in TEP via sonication (Sonica2200ETH, Soltec, Italy) for 30 min. The PVDF powder and the additives were then solubilized in the colloidal solution by magnetic stirring (100 rpm for 8 h). The concentration of TiO_2 catalyst was 0 wt% (M0), 2.5 wt% (M2.5), 5 wt% (M5), and 7 wt% (M7) with respect to PVDF. Table 1 summarizes the polymeric solutions used for membrane preparation.

Before the casting procedure, the solutions were degassed at room temperature (25 °C) for 2 h. The PVDF solutions were cast onto a glass plate using a casting knife (Automatic Film Applicator 4340 by Elcometer, UK) set at 300 μm of thickness. The nascent membranes were subsequently immersed in a coagulation bath of water for 2 h.

The obtained flat membranes were washed with distilled water at 50 °C for 2 h and subsequently with ethanol (2 h) to remove eventual

Table 1
PVDF membranes prepared via NIPS by varying the concentration of TiO_2 in the polymeric solutions.

Membrane	PVDF (wt.%)	TiO_2 (wt.%)	PVP (wt.%)	PEG (wt.%)	TEP (wt.%)
M0	15	0	5	20	60
M2.5	15	0.375	5	20	59.625
M5	15	0.75	5	20	59.25
M7	15	1.05	5	20	58.95

traces of TEP, PVP or PEG. Finally, the membranes were dried overnight at room temperature and 60 °C for 2 h before characterization.

2.4. Membrane characterization

Membrane porosity (ε) was determined according to the gravimetric method consisting of measuring the mass of the membranes in dry and wet circumstances after immersion for 24 h in kerosene and applying the following formula [41]:

$$\varepsilon(\%) = \left\{ \frac{(W_w - W_d)/\rho_i}{(W_w - W_d)/\rho_i + \frac{W_d}{\rho_m}} \right\} \bullet 100 \quad (1)$$

where W_w is the weight of the wet membrane, W_d is the weight of the dry membrane, ρ_i is the kerosene density (0.82 g·cm^{-3}) and ρ_m is the density of the membrane material estimated from the PVDF (1.78 g·cm^{-3}) and TiO_2 (4.23 g·cm^{-3}) densities. Three measurements for each membrane were performed to calculate the average values and standard deviations.

The mean pore size (d_{mean}) and the largest pore size (d_{max}) were assessed using a PMI Capillary Flow Porometer (Model CFP-1500AEXL, Porous Materials Inc., USA) operating via Capwin software (Porous Materials Inc., USA) according to the wet up/dry-up method and using Porewick® (surface tension 16 dyn·cm^{-1}) as the wetting liquid. The experimental data were computed using Caprep software (Porous Materials Inc., USA) to obtain the values of the mean pore diameter (d_{mean}) and the largest pore diameter (d_{max}).

The morphology of the membranes was revealed by a scanning electron microscope (SEM) QUANTA INSPECT F50 (FEI Company, The Netherlands).

Membrane hydrophobicity was estimated by water contact angle (WCA) measurements (Model CAM 200, KSV Instruments, Finland) according to the sessile drop method at ambient temperature.

The Ultraviolet–Visible (UV–Vis) absorption of the photocatalytic membranes was measured using a spectrophotometer (Shimadzu UV-1601, Kyoto, Japan).

The mechanical properties of the membranes were evaluated according to the tensile tests carried out with a single column Universal Testing Machine (Zwick/Roell, model Z2.5, Germany) equipped with a 200 N load cell. Samples of 2.5 cm of length (distance between the clamps of the instruments) and of 1 cm of width were stretched until the breakage at a rate of 25 mm·min^{-1}. The mean values and the standard deviations of the Young's modulus (E_{mod}), the break elongation (ε_{break}) and the tensile strength (R_m) were evaluated on a series of five samples.

2.5. Photocatalytic membrane distillation reactor

The experimental setup for PC-MD is shown in Fig. 1. To explore the synergistic effect of MD and PC, the membranes (active area of 85 cm^2) were allocated in a module equipped with a quartz window to irradiate the membrane surface. The irradiation was provided by a high-pressure UV mercury lamp installed 20 cm above the membrane module and it was characterized by an emission profile between 240 nm and 440 nm, a maximum wavelength of 366 nm and a viewing angle of 90°, which was connected to a 500 W portable power generator.

The feed solution (0.4 L), thermostated at 40, 50, or 60 °C (±0.5 °C) by a Digital Plus Neslab RTE201 thermostatic bath (Thermo Scientific, Italy), was recirculated through the membrane module at a flow rate of 6 L·h^{-1} with a Masterflex L/S digital peristaltic pumps (Cole-Palmer, USA). The initial concentration of As(III) in the feed was 0.06 mg·L^{-1} according to the amount of As revealed in the contaminated groundwater of the Sila Massif (Calabria, Italy) [39]. Experiments were also conducted with As-concentrated solutions (1.00 mg·L^{-1}) to study the kinetic of PC. Thermocouples (Sper Scientific 8000024) were installed at the outlet and inlet of the membrane module to monitor the temperature. Experiments were conducted in a Vacuum Membrane Distillation (VMD) configuration, with the vaporized distillate stripped by a vacuum pump VWR VP 820 (VWR International, US) maintaining the pressure to 2 kPa.

The quality of the permeate was estimated by: i) measuring the conductivity using a YSI Model 3200 conductivity meter at 20 °C (range: 0–4999 μS m^{-1}, accuracy: ±0.50 % full scale); ii) detecting the eventual leakage of TiO_2 NPs from the membrane by Dynamic Light Scattering (DLS) 90Plus Particle Size Analyzer (Brookhaven Instruments Corporation, USA); and iii) estimating the As concentration with HR-CS AAS and analytical kits.

The transmembrane flux was evaluated by recording the weight variations of the feed tank over time using an analytical balance REFLEX HP 8200 (US) with a precision of ± 0.1 g.

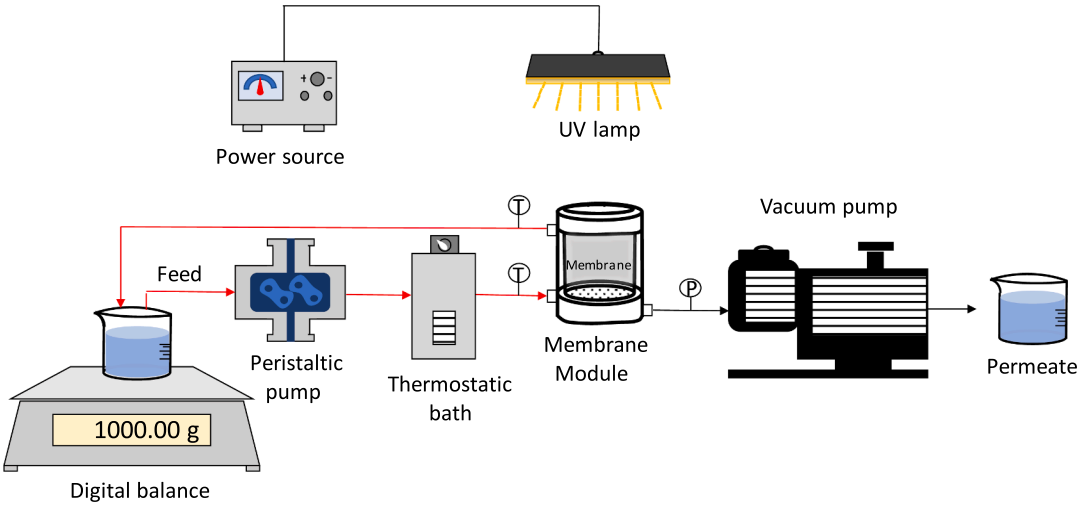

Fig. 1. Schematic representation of the setup for hybridization of VMD with photocatalysis for As remediation.

3. Results

3.1. Membrane characterization

Table 2 summarizes the physical– chemical properties of the lab-made PVDF-based membranes. The membranes presented thicknesses (l) of 105–116 μm and mean pore size (d_{mean}) from 0.123 μm to 0.129 μm, failing in the range of 0.05–0.5 μm typical for MD applications [42]. The largest pore size (d_{max}) ranged from 0.272 μm to 0.288 μm, thus meeting the requirement of MD membranes for a narrow pore size below than 0.5 μm to mitigate the risk of pore wetting [42]. In all cases, the PVDF membranes showed porosities (ε) above 80 % securing minimal resistance to mass transport and modest heat conductivity, both desired in MD to ensure high transmembrane flux and to reduce the impact of temperature polarization [43,44]. These interesting features are attributed to the use of PVP and PEG as additives able to increase the pore size and porosity of the membrane without affecting their homogeneity [45]. With respect to this, several studies reported that the solubilization of appropriate amounts of PVP and PEG in PVDF solutions balances the enhancement of thermodynamic instability of the dope solution (responsible for a high demixing rate with a subsequent increase of the porosity) and the increase of viscosity (slowing the diffusion of the non-solvent into the polymeric solution and mitigating the formation of heterogeneities) [45–47]. Moreover, both PVP and PEG are soluble in water and easily removed from the membrane during the NIPS and washing phases [45–47]. Interestingly, while the presence of TiO_2 NPs in MMMs poorly affected the values of the pore size, the photocatalyst slightly improved the membrane porosity: the value of ε progressively increased from 80.5 ± 1.3 % for bare PVDF membranes (M0) to 83.4 ± 1.4 % for the membrane load with 7 % TiO_2 (M7). This trend could be attributed to the hydrophilic nature of the TiO_2 [48] that facilitates the solvent and non-solvent de-mixing during the NIPS process, leading to superior porosity [49], as clearly observed for PVDF hollow fiber showing an enhancement of the porosity from 35.5 % to 81.4 % with the loading of TiO_2 NPs from 0 wt% to 3 wt% [50].

On the other hand, the presence of the hydrophilic TiO_2 NPs did not compromise the hydrophobicity of the membrane surface; the measurements of the contact angle of the surfaces of the membranes exposed to the atmosphere during the casting process (WCA_{air}) showed values in the range of 93-91°. Furthermore, the surfaces obtained from the cast polymeric solution in contact with the glass in the NIPS process presented a contact angle (WCA_{glass}) of 120 ± 2°.

SEM inspections clarified that the discrepancies in the measurements of the contact angles of the two surfaces are related to differences in terms of morphology (Fig. 2a and b). In general, during the membrane casting, the solvent partially evaporates from the surface of the polymeric solution developing a polymer concentration gradient along the cross section of the nascent membrane resulting in asymmetric structures [51]. According to Smolders et al. [52], finger-like macrovoids are generated by the nuclei of the polymeric lean phase formed below a dense skin top-layer. Strathmann et al. [53] also suggested that the immersion of the cast polymeric solution into the coagulation bath provoked a rapid non-solvent/solvent exchange from the surface in direct contact with the coagulation bath (air surface), inducing the formation of a finger-like morphology (Fig. 2.c) [54]. On the other hand, the slow permeation (i.e., diffusion) of the non-solvent (i.e., water of the coagulation bath) into the nascent membrane delayed the demixing on the opposite surface (glass surface), resulting in a sponge-like morphology (Fig. 2.d) [55].

The latter morphology is usually characterized by superior roughness, which increases the apparent contact angle, as predicted by Wenzel [56,57]. Based on this superior hydrophobic behaviour, the bottom surface is more appropriate to be in contact with the feed solution in VMD experiments, thus limiting the wetting phenomena [58]. Moreover, TiO_2 NPs did not affect the membrane morphologies, and the NPs were clearly embedded into the polymeric network, especially visible with the backscattered electron detector (BSED) in Fig. 2.d and detected with SEM-EDX (Figure S1 and Table S1). Additionally, analytical analysis proved the absence of leaked TiO_2 NPs in the coagulation and washing baths, confirming their proper embodiment.

UV–Vis spectra of photocatalytic membranes reported in Fig. 3 showed that the embodiment of TiO_2 NPs notably increased the absorbance intensities in the UV region. While PVDF membranes did not absorb radiation for wavelengths above 250 nm, the presence of the semiconductor photocatalyst conferred to the polymer a wide absorption band in the range from 250 nm to 400 nm with a maximum at ca. 320 nm, coherently with the electronic transitions associated with the energy gap of TiO_2 [59]. Interestingly, the intensity of the band progressively increased with the concentration of the TiO_2 NPs up to 5 wt%, whereas a minimal improvement was observed by increasing the concentration of the photocatalyst from 5 wt% (M5) to 7 wt% (M7). This is probably related to the fact that a high concentration of the photocatalytic fillers promoted the formation of aggregates (insert of Fig. 3) with a successive reduction of the active surface available for light absorption.

Table 2
Summary of membrane characterizations.

Membrane	l (μm)	d_{mean} (μm)	d_{max} (μm)	ε (%)	WCA_{Air} (°)	WCA_{Glass} (°)
M0	116 ± 2	0.127 ± 0.006	0.272 ± 0.002	80.5 ± 1.3	93 ± 2	122 ± 2
M2.5	105 ± 3	0.129 ± 0.004	0.278 ± 0.004	81.9 ± 1.0	93 ± 2	120 ± 4
M5	109 ± 2	0.124 ± 0.005	0.288 ± 0.008	83.1 ± 1.5	93 ± 2	118 ± 5
M7	108 ± 3	0.123 ± 0.006	0.284 ± 0.008	83.4 ± 1.4	91 ± 2	119 ± 4

3.2. VMD performance

VMD tests using As-contaminated distilled water ([As(III)] = 0.06 $mg{\cdot}L^{-1}$) as feed (flow rate = 6 $L{\cdot}h^{-1}$) were performed at different temperatures. The values reported in Fig. 4.a and b are the mean values of the flux observed over 6 h of experiments. The transmembrane flux measured for the MMM embedding 7 wt% of the photocatalyst (M7) increased from 1.3 ± 0.1 $kg{\cdot}m^{-2}{\cdot}h^{-1}$ to 6.3 ± 0.3 $kg{\cdot}m^{-2}{\cdot}h^{-1}$ by raising the feed temperature from 40 °C to 60 °C in the absence of UV irradiation (Lamp off). This behavior is a consequence of the exponential increase of the vapor pressure at the feed interface (p^{feed}) with the temperature (T^{feed}) [60], positively affecting the transmembrane flux (J) expressed as:

$$J = K(p^{feed} - p^{vacuum}) \quad (2)$$

where p^{vacuum} is the vacuum pressure in the distillate compartment (2 kPa) and K is an empirical constant. In fact, the value of p^{feed} increased from 7.38 kPa at 40 °C to 19.95 kPa at 60 °C, as determined by the Antonie equation [61].

According to Fig. 4.a, the presence of UV irradiation (Lamp on), employed to activate the photocatalyst, boosted the water vaporization rate over the entire range of the investigated temperatures. This behavior is due to the radiant heating power of the UV radiation absorbed by the VMD cell, estimated to be about 10^4 $W{\cdot}m^{-2}$. Feeding water at 60 °C in the absence of UV irradiation, the temperature of the retentate at the outlet of the membrane module was 57.9 °C as a consequence of heat losses by conduction across the membrane and by latent heat of vaporization associated with the transmembrane flux [62]. On the other hand, when the UV lamp was turned on, the additional radiative heat raised the outlet temperature of the retentate stream to 61.4 °C, leading to a transmembrane flux enhancement of ca. 12.7 %. Analogous impacts were observed for all the developed membranes

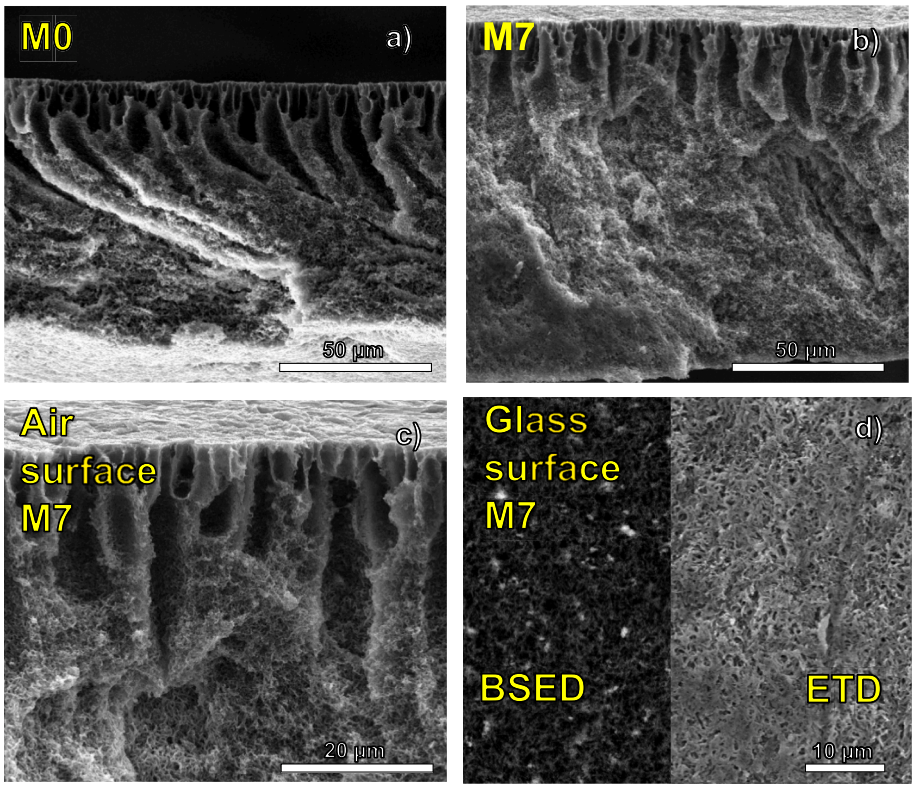

Fig. 2. a) Cross section of bare PVDF membrane (M0) at a magnification of 2,000; b) cross section of PVDF membrane doped with 7 wt% of TiO_2 NPs (M7) at a magnification of 2,000; c) zoom of the cross section of the air surface of M7 at a magnification of 5,000; d) glass surface of M7 observed with backscattered electron detector (left) and Everhart– Thornley detector (ETD).

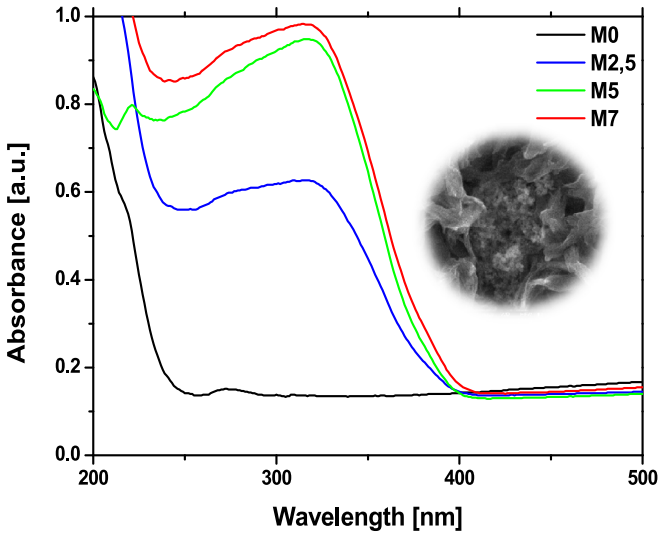

Fig. 3. UV–Vis spectra and details of an aggregate of TiO_2 NPs in a PVDF membrane doped with 7 wt% of TiO_2 NPs (M7) observed by SEM at a magnification of 100,000 (insert).

(Figure S2).

Likewise, the experiments under UV irradiation were completed (6 h) without flux deterioration, confirming the stability of the photocatalytic MMMs even in the case of high TiO_2 loading (M7).

In all cases, the concentration of As(III) in the distillate after 6 h of VMD practice was below to detection limit of analytical methodologies (0.005 mg·L^{-1}) confirming the potentialities of VMD in producing high-quality distilled water from contaminated As aqueous solutions, even below the rigorous WHO drinking water standard.

Interestingly, the presence of the TiO_2 NPs had a poor impact on the VMD performance of the PVDF-based membranes (Fig. 4b and Figure S2): the impact of the variation of the TiO_2 NP content from 0 wt % (M0) to 7 wt% (M7) on the transmembrane flux was below 10 %; this was due to the modest impact of the photocatalyst on the morphological and chemical-physical properties of PVDF membranes (Table 2).

Although the presence of UV irradiation increased the VMD productivity (transmembrane flux raised of the 12.7 % at an inlet feed temperature of 60 °C), the employment of the highly energy intensive lamp drastically increased the specific energy consumption of the process (in the order of 10^4 KWh·m^{-3}). This suggested that the treatment of diluted As-contaminated solutions with UV radiation is not feasible from an energetic point of view, highlighting the need for the use of an upstream process for the dehydration of the feed before As remediation. From this perspective, the developed photocatalytic MMMs could be used in two consecutive stages: i) a preliminary VMD step in the absence of UV irradiation aimed at recovering large amounts of water while concentrating As; and ii) a second PC-VMD step under UV irradiation to convert As(III) into As(V), which can be subsequently removed by filtration through absorbent media.

Fig. 5 clarifies the capabilities of VMD in the recovery of water from the As-contaminated aqueous solution. The lowest performance was recorded at a feed inlet temperature of 40 °C when only 17.8 % (Fig. 5.a) of the water was recovered after 6 h due to the relatively low transmembrane flux (1.3 kg·m^{-2}·h^{-1}); this provoked a minimal improvement of the concentration of As in the retentate from 0.06 mg·L^{-1} to 0.07 mg·L^{-1} (Fig. 5.b). The enhancement of the transmembrane flux to 6.3 kg·m^{-2}·h^{-1} by raising the feed inlet temperature to 60 °C improved the water recovery factor up to 80.5 % (Fig. 5.a), with a consequent increase in the As concentration from 0.06 mg·L^{-1} to 0.31 mg·L^{-1}(Fig. 5.b).

The transmembrane flux was not dependent on the As(III) concentration; for instance, the transmembrane flux of M7 exhibited a modest

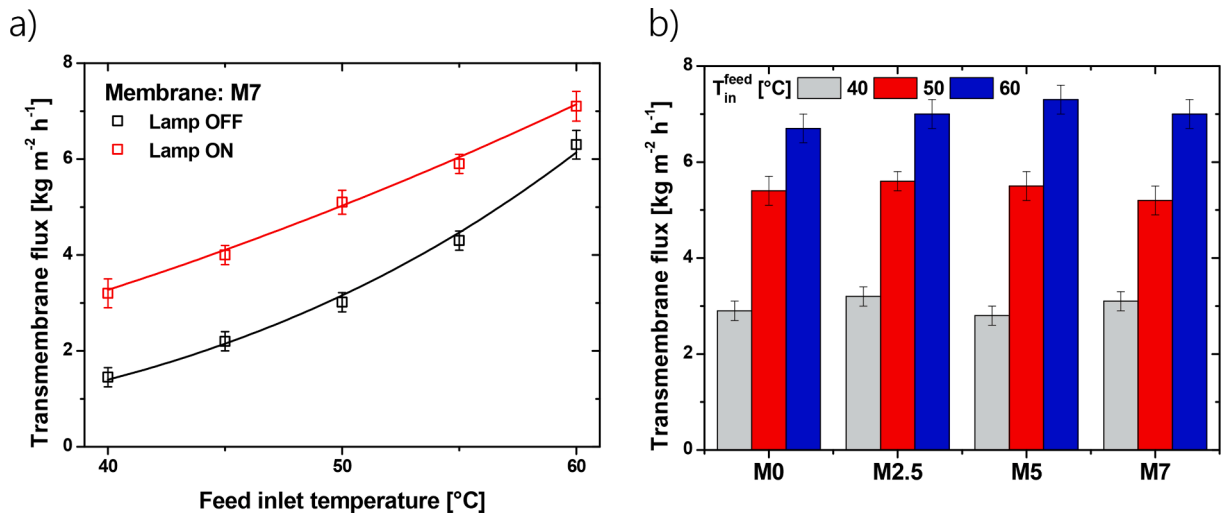

Fig. 4. a) Average transmembrane fluxes of MMM loaded with 7 wt% of TiO_2 NPs (M7) in VMD experiments in the presence (Lamp ON) or absence (Lamp OFF) of UV irradiation at different feed temperatures; b) Transmembrane fluxes of PVDF membranes with different loadings of TiO_2 NPs in the presence (Lamp ON) of UV irradiation at different feed temperature.

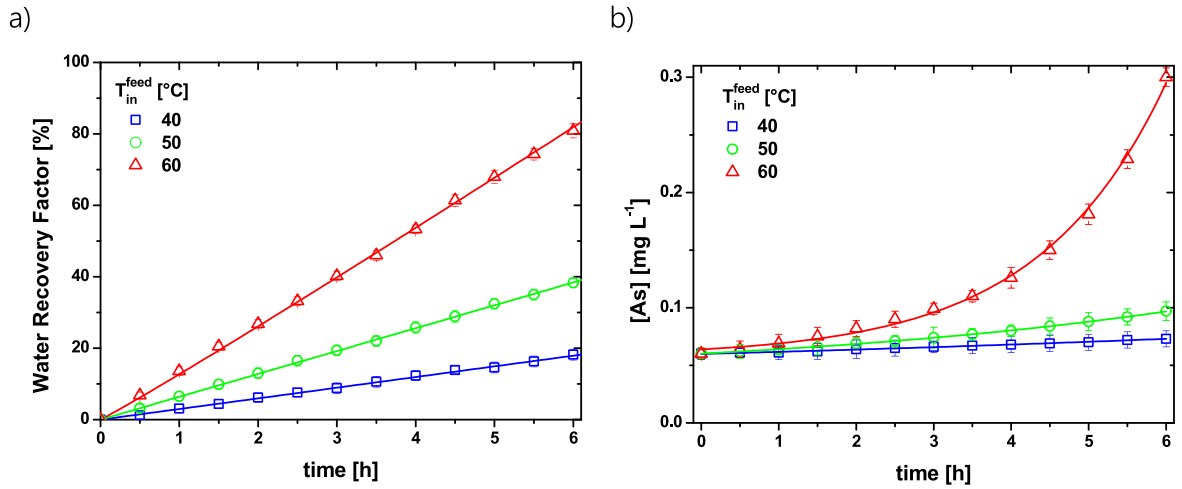

Fig. 5. A) water recovery factor and b) evolution of as concentration in the retentate stream during 6 h of VMD experiments carried out with M7 membrane at different feed temperatures in the absence of UV irradiation.

variation of 6 % despite the As concentration being raised 5-folds. This is due to the low sensitivity of the MD process to the solute concentration in the diluted solution. As per Raoult's equation, the vapor pressure of the feed solution (p^{feed}) depends on the vapor pressure of pure water (p_0^{feed}), the molar fraction (x_w), and the activity coefficient (γ_w) of water:

$$p^{feed} = p_0^{feed} \bullet x_w \bullet \gamma_w \quad (3)$$

In the case of the diluted solution, both x_w and γ_w tend toward 1 making p^{feed} close to p_0^{feed}.

DLS and HR-CS AAS analysis of both permeate and retentate confirmed the absence of leakage phenomenon of the TiO_2 NPs from the membranes to the aqueous phases.

3.3. Photocatalytic membranes for As(III) oxidation in As(V)

To assess the photocatalytic performance of the lab-made MMMs, an aqueous solution of As(III) of 1.00 $mg{\cdot}L^{-1}$ was recirculated for 3 h to the membrane module in the presence of UV radiation at different inlet temperatures. As expected, the bare PVDF membrane (M0) was found to be ineffective in the photo-oxidation of As leading to an improvement of the As(III) concentration coherent with the dehydration of the solution (Fig. 6.a). On the other hand, a substantial reduction in As(III) concentration was observed for the PVDF membranes doped with TiO_2 NPs. Using M2.5, the arsenite concentration decreased to 0.71 $mg{\cdot}L^{-1}$ at 40 °C, whereas almost 50 % of As(III) was converted into arsenate at 60 °C (Fig. 6.b). The increase of the TiO_2 content incorporated into the PVDF matrix to 5 wt% (M5) increased the photocatalytic performance, leading to a reduction of As(III) concentration to 0.28 $mg{\cdot}L^{-1}$ at 60 °C. The best performance was observed for the membrane with the highest loading of the catalyst: M7 decreased the concentration of arsenite to 0.44 $mg{\cdot}L^{-1}$ at 40 °C and further decreased it to 0.09 $mg{\cdot}L^{-1}$ when the temperature was increased to 60 °C.

In general, higher feed temperatures increase the rate of the photocatalytic reaction. When TiO_2 NPs are irradiated with radiation matching their band gap, electron– hole (e^{-}-h^{+}) pairs are generated in the conduction and valence bands [63]. In an aqueous system, h^{+} easily reacts with H_2O, leading to the generation of $OH^{\bullet}$ radicals consisting of highly oxidizing species [64]. Higher temperatures of the reaction system (aqueous medium where the reaction occurs) improve the mobility of the e^{-}-h^{+} pairs photogenerated by the semiconductor materials. In fact, several studies have demonstrated that temperatures above 80 °C

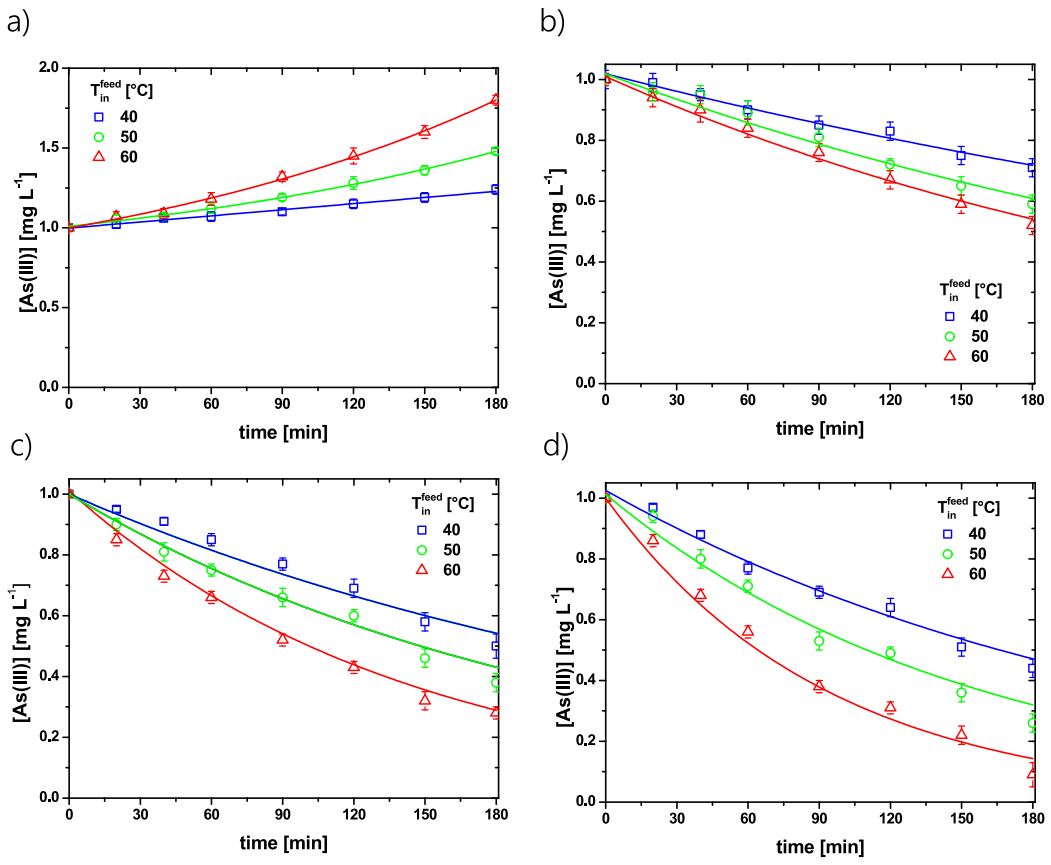

Fig. 6. Time evolution of the As(III) concentration in PC-VMD tests at different temperatures carried out with: a) M0, b) M2.5, c) M5, and d) M7 membranes.

limit the photo-oxidation activity of TiO_2 NPs by favoring the recombination of the e^--h^+ pairs [65], while in the range of 20–70 °C, the photocatalytic activity increases with temperature [65,66], which is consistent with our observations. These materials being photothermal-photocatalytic are also capable of absorbing photons and simultaneously generate heat by dissipating it to the environment, which would lead to the acceleration of the photocatalytic reaction by increasing the mobility of charge carriers in the material [67].

In all cases, the concentration of arsenite during the experiment exponentially decreased according to a first-order kinetics ($R^2 > 0.96$) [68,69]:

$$[As(III)]_t = [As(III)]_0 \bullet \exp(-kt) \quad (4)$$

where $[As(III)]_0$ is the initial arsenite concentration (1 mg·L^{-1}), $[As(III)]_t$ is the concentration of As(III) at the generic irradiation time t, and k is the experimentally observed first-order kinetic constant. The value of k increased with the concentration of the photocatalyst from 0.0019 min^{-1} for M2.5 to 0.0034 min^{-1} for M5 achieving 0.0044 min^{-1} for M7 (feed inlet temperature of 40 °C). As expected in view of the UV–Vis spectra (Fig. 3) and the aggregates observed for M7, the value of k does not increase proportionally to the amount of TiO_2 loaded in the membrane.

The value of k also raised with feed temperature, reaching a maximum value of 0.0106 min^{-1} for M7 at 60 °C; one order of magnitude lower than the one (k = 0.123 min^{-1}) observed for a colloidal dispersion of 0.05 g·L^{-1} of TiO_2 NPs in water containing an initial concentration of arsenate of 0.5 mg·L^{-1} [37]. This is due to the direct contact of the photocatalyst with the contaminant solubilized in water, facilitating photo-oxidation. Although the superior effectiveness of the suspension of the TIO_2 NPs in the As-contaminated aqueous solution with respect to their embodiment into the membrane, the submicrometric sizes of the photocatalyst imposes sophisticated and expensive strategies for its separation and recovery from the treated water, hindering the feasibility at large scale [70].

The benefits of the photo-oxidation were corroborated by the filtration of the treated solutions with aluminosilicate-based absorbent media able to effectively remove the oxidized state of As, while As(III) was not absorbed (Figure S3).

3.4. PC-VMD for as remediation

The efficiency of the photocatalytic membranes for treating As-contaminated solutions was evaluated by performing a first stage of VMD (lasting 4.5 h) followed by a second stage of PC-VMD (lasting 1.5 h) employing the membrane loaded with 7 wt% of TiO_2 (M7). To evaluate the eventual interference of other ions, experiments were conducted by feeding a sample of real water to the membrane module (feed inlet temperature of 60 °C) with the composition reported in Table 3.

The transmembrane flux in the absence of UV irradiation was 6.1 ± 0.2 kg·m^{-2}·h^{-1}. As predicted by Equation (3), the presence of ions poorly affected the evaporation rate: a reduction of less than 3 % was observed in the VMD experiments with respect to the experiments conducted with distilled water contaminated by As (0.06 mg·L^{-1}). The conventional VMD operation allowed the recovery of 58.3 % of water, raising the concentration of As(III) in the retentate to 0.15 mg·L^{-1}, while As(V) was absent in the retentate stream (Fig. 7).

In the subsequent 1.5 h of PC-VMD (Lamp ON), the heat transferred by the irradiation to the membrane module resulted in an improvement of the transmembrane flux to 7.1 ± 0.2 kg·m^{-2}·h^{-1} increasing the water recovery factor up to 80.9 %.

On the other hand, the exposure of M7 to UV light activated the photocatalyst embedded in the PVDF microporous membrane. Therefore, despite the dehydration of the feed concentrated the As species to

Table 3
Ionic composition of a real water sample (major ions are reported).

Ion	HCO_3^-	Cl^-	Na^+	Ca^{2+}	SO_4^{2-}	Mg^{2+}	K^+	NO_3^-	F^-	As(III)
$mg{\cdot}L^{-1}$	30.9	10.1	9.7	30.9	10.1	1.4	0.6	0.1	0.1	0.06

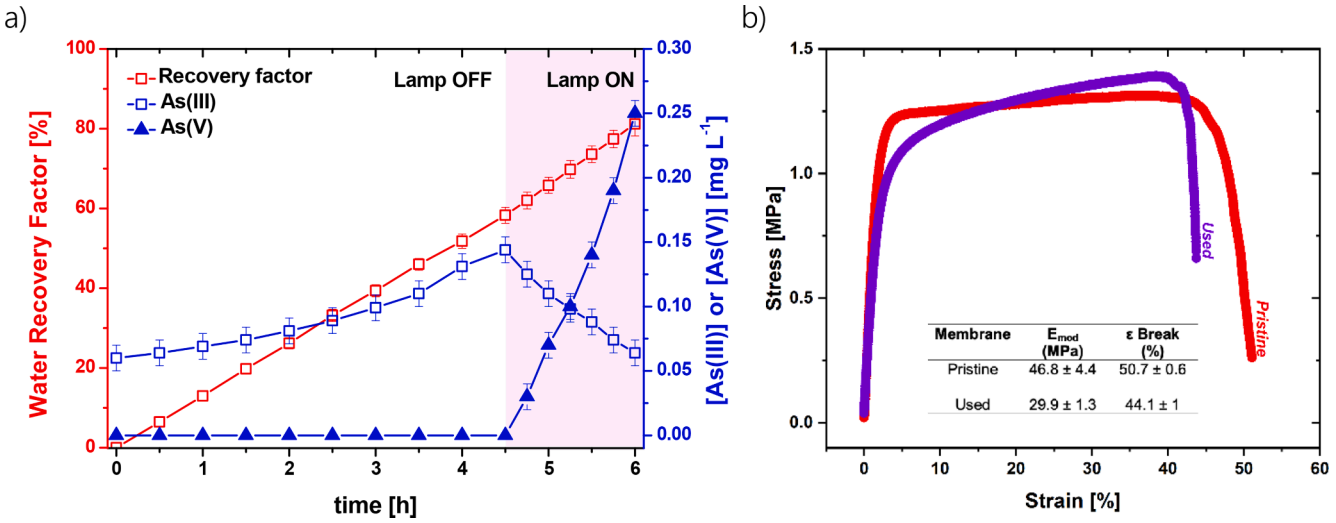

Fig. 7. a) Evolution of the recovery factor and As(III) and As(V) concentrations in experiments of conventional VMD followed by PC-VMD (Lamp ON) carried out at 60 °C with M7 using multi-ion solution contaminated by As (0.06 $mg{\cdot}L^{-1}$) as feed. b) Mechanical properties of M7 before (pristine) and after five cycles of PC-VMD (used).

0.31 $mg{\cdot}L^{-1}$, the concentration of As(III) progressively reduced from 0.15 $mg{\cdot}L^{-1}$ to 0.06 $mg{\cdot}L^{-1}$ coupled with an improvement of As(V) concentration to 0.25 $mg{\cdot}L^{-1}$.

The photo-oxidation of As(III) to As(V) was in agreement with the first-order kinetics reported in Equation (4), but the value of k reduced from 0.0106 min^{-1} to 0.0071 min^{-1}. This effect is mostly related to the presence of bicarbonate ions interfering with the photo-oxidation process. In fact, HCO_3^- ions compete with As(III), especially with hydroxyl radicals [71]. Thus, the treatment of a real solution could require an early stage treatment to remove the HCO_3^- ions [72].

After five cycles of PC-VMD experiments, a *post-hoc* characterization was conducted to assess the impact of the long-term exposure to the UV irradiation on the mechanical stability of M7. As reported in Fig. 7.b, PC-VMD experiments poorly impacted on the mechanical resistance of the membranes since both pristine and used membranes demonstrated tensile strengths (R_m) failing in the range of 1.3–1.4 MPa. Nevertheless, the used membranes showed a minor reduction of elastic properties visible by the decrease with respect to the pristine membrane of both the Young Modulus (E_{mod}) from 46.8 MPa to 29.9 MPa and the elongation at break (ε_{break}) from 50.7 % to 44.6 %. The moderate temperature of MD process was insufficient to induce any detrimental thermal effect on the membrane compromising its mechanical stability (PVDF melting point occurs at temperature above 160 °C [73]). Thus, the observed embrittlement of the membrane was caused by UV radiation able to promote oxidation reactions, chain-scissions and decompositions of PVDF [74–76]. The embrittlement phenomenon highlights the inherent challenges associated with the limited long-term stability of polymeric membranes when exposed to UV irradiation. Moving forward, future studies will focus on exploring novel approaches such as employing UV-resistant supports and utilizing solar-activated photocatalysts to address the stability issues encountered in UV-activated PVDF-based photocatalytic membranes.

4. Conclusions

This work proposed a novel integrated MD and photo-oxidation process by doping microporous hydrophobic PVDF membranes with TiO_2 NPs, enabling the simultaneous recovery of high-quality freshwater and the conversion of As(III) into As(V), the latter being less toxic and easily removed with well-established technologies.

MMMs were prepared according to the NIPS protocol using TEP as the green solvent in a dispersion of TiO_2 NPs where PVDF was solubilized. Additives (PEG and PVDF) ensured the fabrication of highly porous membranes ($\varepsilon > 80$ %) with a narrow pore size (d_{mean} in the range of 0.123–0.129 μm and largest pore below to 0.288 μm). Likewise, the membranes presented an asymmetric structure with a finger-like top layer on a spherulitic structure. This caused an asymmetry in hydrophobicity because the superior roughness of the spherulitic structure raised the contact angles to 120 ± 2°, whereas a contact angle of 92 ± 1° was observed for the smoother surface with a finger-like morphology.

Notably, the increase in the TiO_2 NP concentration from 0 wt% (M0) to 7 wt% (M7) did not affect the morphological properties of the membrane, despite the aggregates observed for the MMMs with the highest loading of the photocatalyst (M7). On the other hand, the enhancement of the TiO_2 content increased the absorbance in the UV region of the spectrum.

VMD experiments demonstrated the ability of the lab-made photocatalytic MMMs to recover more than 80 % of water from As contaminates solution, enhancing the concentration of As(III) 5-folds. Moreover, the transmembrane flux raised from 1.2 ± 0.1 $kg{\cdot}m^{-2}{\cdot}h^{-1}$ to 6.3 ± 0.3 $kg{\cdot}m^{-2}{\cdot}h^{-1}$ when increasing the feed temperature from 40 °C to 60 °C in the absence of UV irradiation. By switching on the UV lamp, the flux further increased to 7.1 ± 0.2 $kg{\cdot}m^{-2}{\cdot}h^{-1}$ (inlet feed temperature of 60 °C) due to the radiant heating power of the UV radiation. Likewise, M7 membranes were able to photo-oxidize As(III) to As(V) under UV irradiation with a first-order kinetic constant of 0.0106 min^{-1} at 60 °C. However, because of the higher energy consumption of the UV lamp, it is convenient to exploit the photocatalytic properties of the membranes to treat As concentrated solutions.

The potential of the novel membrane technology was assessed by treating real water in two consecutive stages: i) VMD (4.5 h) to recover 58.3 % of the water concentrating As(III) up to 0.15 $mg{\cdot}L^{-1}$; and ii) PC-

VMD under UV light (1.5 h) to intensify the recovery of water up to 80 % and to ensure the abatement of the concentration of As(III) to 0.06 mg·L^{-1} via its photo-oxidation into As(V), the latter effortlessly removed by filtration with alluminosilicates.

Post-hoc mechanical test on M7 employed in 5 cycles of PC-VMD (total irradiation time: 7.5 h) revealed the emergence of polymer embrittlement induced by the UV radiation. These findings underscore the pressing need for the development of photocatalytic membranes with long-term stability.

Overall, this work demonstrated the advantages of combining MD and photo-oxidation in a single process by employing green hydrophobic microporous membranes with photocatalytic properties that are exploitable for continuous and intensified remediation of As -contaminated waterbodies.

CRediT authorship contribution statement

Sergio Santoro: Writing – review & editing, Writing – original draft, Supervision, Methodology, Conceptualization. **Jessica Occhiuzzi:** Investigation, Data curation. **Marco Aquino:** Methodology, Investigation. **Antonio Politano:** Validation, Supervision. **Salvatore Straface:** Supervision, Resources. **Giuseppe D'Andrea:** Investigation. **Cristobal Carrillo:** Investigation. **Reyes Mallada:** Writing – review & editing, Supervision, Conceptualization. **Andreina Garcia:** Writing – review & editing. **Humberto Estay:** Writing – review & editing. **Dimitrios Xevgenos:** Writing – review & editing. **Pietro Argurio:** Validation, Supervision, Conceptualization. **Efrem Curcio:** Writing – review & editing, Writing – original draft, Supervision.

Declaration of competing interest

The authors declare the following financial interests/personal relationships which may be considered as potential competing interests: [Salvatore Straface reports financial support was provided by European Union. Andreina Garcia, Humberto Estay reports financial support was provided by National Research and Development Agency. If there are other authors, they declare that they have no known competing financial interests or personal relationships that could have appeared to influence the work reported in this paper].

Acknowledgments

The financial support of: the European Union through the project H2020-MSCA-RISE REMIND "Renewable Energies for Water Treatment and REuse in Mining Industries" (Grant agreement ID: 823948), and the National Research and Development Agency ANID (former CONICYT) through the AMTC Basal Project - Basal Financing Program for Scientific and Technological Centers - grant numbers AFB220002/AFB230001 and FONDECYT Regular - grant number 1220088 are kindly acknowledged.

Appendix A. Supplementary material

Supplementary material to this article can be found online at https://doi.org/10.1016/j.seppur.2024.127042.

References

[1] Agency for Toxic Substances and Disease Registry (ATSDR), Priority list of hazardous substances, (n.d.). https://www.atsdr.cdc.gov/spl/index.html#2022spl (accessed April 1, 2023).
[2] World Health Organization's (WHO), World Health Organization. Guidelines for Drinking-Water Quality, 2017.
[3] K. Khanna, S.K. Kohli, P. Kumar, P. Ohri, R. Bhardwaj, P. Alam, P. Ahmad, Arsenic as hazardous pollutant: perspectives on engineering remediation tools, Sci. Total Environ. 838 (2022) 155870, https://doi.org/10.1016/j.scitotenv.2022.155870.
[4] P. Bhattacharya, A.H. Welch, K.G. Stollenwerk, M.J. McLaughlin, J. Bundschuh, G. Panaullah, Arsenic in the environment: biology and chemistry, Sci. Total Environ. 379 (2007) 109–120, https://doi.org/10.1016/j.scitotenv.2007.02.037.
[5] S. Bhowmick, B. Nath, D. Halder, A. Biswas, S. Majumder, P. Mondal, S. Chakraborty, J. Nriagu, P. Bhattacharya, M. Iglesias, G. Roman-Ross, D. G. Mazumder, J. Bundschuh, D. Chatterjee, Arsenic mobilization in the aquifers of three physiographic settings of West Bengal, India: understanding geogenic and anthropogenic influences, J. Hazard. Mater. 262 (2013) 915–923, https://doi.org/10.1016/j.jhazmat.2012.07.014.
[6] S. Quazi, D. Sarkar, R. Datta, Human health risk from arsenical pesticide contaminated soils: a long-term greenhouse study, J. Hazard. Mater. 262 (2013) 1031–1038, https://doi.org/10.1016/j.jhazmat.2012.10.027.
[7] J.O. Nriagu, P. Bhattacharya, A.B. Mukherjee, J. Bundschuh, R. Zevenhoven, R.H. Loeppert, Arsenic in soil and groundwater: an overview, in: Arsen. Soil Groundw. Environ., Elsevier, 2007: pp. 3–60. 10.1016/S1875-1121(06)09001-8.
[8] S. Santoro, H. Estay, A.H. Avci, L. Pugliese, R. Ruby-Figueroa, A. Garcia, M. Aquino, S. Nasirov, S. Straface, E. Curcio, Membrane technology for a sustainable copper mining industry: the chilean paradigm, Clean. Eng. Technol. 2 (2021) 100091, https://doi.org/10.1016/j.clet.2021.100091.
[9] A.K. Sharma, J.C. Tjell, J.J. Sloth, P.E. Holm, Review of arsenic contamination, exposure through water and food and low cost mitigation options for rural areas, Appl. Geochemistry. 41 (2014) 11–33, https://doi.org/10.1016/j.apgeochem.2013.11.012.
[10] R. Singh, S. Singh, P. Parihar, V.P. Singh, S.M. Prasad, Arsenic contamination, consequences and remediation techniques: a review, Ecotoxicol. Environ. Saf. 112 (2015) 247–270, https://doi.org/10.1016/j.ecoenv.2014.10.009.
[11] S. Santoro, A.H. Avci, M. Aquino, L. Pugliese, S. Straface, E. Curcio, Towards the Global Rise of Zero Liquid Discharge for Wastewater Management: The Mining Industry Case in Chile, in: Springer Berlin Heidelberg, Berlin, Heidelberg, 2021: pp. 1–14. 10.1007/698_2021_785.
[12] S. Radić, H. Crnojević, V. Vujčić, G. Gajski, M. Gerić, Ž. Cvetković, C. Petra, V. Garaj-Vrhovac, V. Oreščanin, Toxicological and chemical assessment of arsenic-contaminated groundwater after electrochemical and advanced oxidation treatments, Sci. Total Environ. 543 (2016) 147–154, https://doi.org/10.1016/j.scitotenv.2015.10.158.
[13] R. Molinari, P. Argurio, Arsenic removal from water by coupling photocatalysis and complexation-ultrafiltration processes: a preliminary study, Water Res. 109 (2017) 327–336, https://doi.org/10.1016/j.watres.2016.11.054.
[14] L. Yin, L. Liu, S. Lin, G. Owens, Z. Chen, Synthesis and characterization of nanoscale zero-valent iron (nZVI) as an adsorbent for the simultaneous removal of AS(III) and as(v) from groundwater, J. Water Process Eng. 47 (2022) 102677, https://doi.org/10.1016/j.jwpe.2022.102677.
[15] B.S. Rathi, P.S. Kumar, A review on sources, identification and treatment strategies for the removal of toxic arsenic from water system, J. Hazard. Mater. 418 (2021) 126299, https://doi.org/10.1016/j.jhazmat.2021.126299.
[16] J. Ryu, W. Choi, Effects of TiO2 surface modifications on photocatalytic oxidation of arsenite: the role of superoxides, Environ. Sci. Technol. 38 (2004) 2928–2933, https://doi.org/10.1021/es034725p.
[17] K.K. Sirkar, A.G. Fane, R. Wang, S.R. Wickramasinghe, Process intensification with selected membrane processes, Chem. Eng. Process. Process Intensif. 87 (2015) 16–25, https://doi.org/10.1016/j.cep.2014.10.018.
[18] T. Guo, J. Englehardt, T. Wu, Review of cost versus scale: water and wastewater treatment and reuse processes, Water Sci. Technol. 69 (2013) 223–234, https://doi.org/10.2166/wst.2013.734.
[19] S. Mondal, M. Malankowska, A.H. Avci, U.T. Syed, L. Upadhyaya, S. Santoro, Chapter 10 - membrane sensors for pollution problems, in: A. Basile, M. Gensini, I. Allegrini, A. Figoli (Eds.), Curr. Trends Futur, Dev. Membr., Elsevier, 2023, pp. 335–361, https://doi.org/10.1016/B978-0-12-824103-5.00004-8.
[20] F.E. Ahmed, R. Hashaikeh, N. Hilal, Hybrid technologies: the future of energy efficient desalination – a review, Desalination 495 (2020) 114659, https://doi.org/10.1016/j.desal.2020.114659.
[21] M. Bassyouni, M.H. Abdel-Aziz, M.S. Zoromba, S.M.S. Abdel-Hamid, E. Drioli, A review of polymeric nanocomposite membranes for water purification, J. Ind. Eng. Chem. 73 (2019) 19–46, https://doi.org/10.1016/j.jiec.2019.01.045.
[22] S. Santoro, M. Aquino, C. Rizza, J. Occhiuzzi, D. Mastrippolito, G. D'Olimpio, A. H. Avci, J. De Santis, V. Paolucci, L. Ottaviano, L. Lozzi, A. Ronen, M. Bar-Sadan, D. S. Han, A. Politano, E. Curcio, Lithium recovery through WS2 nanofillers-promoted solar photothermal membrane crystallization of LiCl, Desalination 546 (2023) 116186, https://doi.org/10.1016/j.desal.2022.116186.
[23] I. Ounifi, Y. Guesmi, C. Ursino, S. Santoro, S. Mahfoudhi, A. Figoli, E. Ferjanie, A. Hafiane, Antifouling membranes based on cellulose acetate (CA) blended with poly(acrylic acid) for heavy metal remediation, Appl. Sci. 11 (2021), https://doi.org/10.3390/app11104354.
[24] N. Abdullah, N. Yusof, W.J. Lau, J. Jaafar, A.F. Ismail, Recent trends of heavy metal removal from water/wastewater by membrane technologies, J. Ind. Eng. Chem. 76 (2019) 17–38, https://doi.org/10.1016/j.jiec.2019.03.029.
[25] C. Algieri, V. Pugliese, G. Coppola, S. Curcio, V. Calabro, S. Chakraborty, Arsenic removal from groundwater by membrane technology: advantages, disadvantages, and effect on human health, Groundw. Sustain. Dev. 19 (2022) 100815, https://doi.org/10.1016/j.gsd.2022.100815.
[26] L. Eykens, K. De Sitter, C. Dotremont, L. Pinoy, B. Van Der Bruggen, How to optimize the membrane properties for membrane distillation: a review, Ind. Eng. Chem. Res. 55 (2016) 9333–9343, https://doi.org/10.1021/acs.iecr.6b02226.
[27] A.H. Avci, S. Santoro, A. Politano, M. Propato, M. Micieli, M. Aquino, Z. Wenjuan, E. Curcio, Photothermal sweeping gas membrane distillation and reverse

electrodialysis for light-to-heat-to-power conversion, Chem. Eng. Process. - Process Intensif. 164 (2021) 108382, https://doi.org/10.1016/j.cep.2021.108382.
[28] S. Abramovich, D. Dutta, C. Rizza, S. Santoro, M. Aquino, A. Cupolillo, J. Occhiuzzi, M.F. La Russa, B. Ghosh, D. Farias, A. Locatelli, D.W. Boukhvalov, A. Agarwal, E. Curcio, M. Bar Sadan, A. Politano, NiSe and CoSe topological nodal-line semimetals: a sustainable platform for efficient thermoplasmonics and solar-driven photothermal membrane distillation, Small 18 (2022) 2201473, https://doi.org/10.1002/smll.202201473.
[29] N. Thomas, M.O. Mavukkandy, S. Loutatidou, H.A. Arafat, Membrane distillation research & implementation: lessons from the past five decades, Sep. Purif. Technol. 189 (2017) 108–127, https://doi.org/10.1016/j.seppur.2017.07.069.
[30] A.E. Kabeel, M. Abdelgaied, E.M.S. El-Said, Study of a solar-driven membrane distillation system: evaporative cooling effect on performance enhancement, Renew. Energy. 106 (2017) 192–200, https://doi.org/10.1016/j.renene.2017.01.030.
[31] F. Macedonio, E. Curcio, E. Drioli, Integrated membrane systems for seawater desalination: energetic and exergetic analysis, economic evaluation, experimental study, Desalination 203 (2007) 260–276, https://doi.org/10.1016/j.desal.2006.02.021.
[32] M.M. Damtie, R.H. Hailemariam, Y.C. Woo, K.-D. Park, J.-S. Choi, Membrane-based technologies for zero liquid discharge and fluoride removal from industrial wastewater, Chemosphere 236 (2019) 124288, https://doi.org/10.1016/j.chemosphere.2019.07.019.
[33] N.M.A. Omar, M.H.D. Othman, Z.S. Tai, A.O.A. Amhamed, T.A. Kurniawan, M. H. Puteh, M.N.M. Sokri, Recent progress, bottlenecks, improvement strategies and the way forward of membrane distillation technology for arsenic removal from water: a review, J. Water Process Eng. 52 (2023) 103504, https://doi.org/10.1016/j.jwpe.2023.103504.
[34] S. Santoro, M. Aquino, C. Rizza, A. Cupolillo, D.W. Boukhvalov, G. D'Olimpio, S. Abramovich, A. Agarwal, M.B. Sadan, A. Politano, E. Curcio, Plasmonic nanofillers-enabled solar membrane crystallization for mineral recovery, Desalination 563 (2023) 116730, https://doi.org/10.1016/j.desal.2023.116730.
[35] S. Santoro, A.H. Avci, A. Politano, E. Curcio, The advent of thermoplasmonic membrane distillation, Chem. Soc. Rev. 51 (2022) 6087–6125, https://doi.org/10.1039/D0CS00097C.
[36] Y. Choi, G. Naidu, L.D. Nghiem, S. Lee, S. Vigneswaran, Membrane distillation crystallization for brine mining and zero liquid discharge: opportunities{,} challenges{,} and recent progress, Environ. Sci. Water Res. Technol. 5 (2019) 1202–1221, https://doi.org/10.1039/C9EW00157C.
[37] S. Santoro, P. Timpano, A.H. Avci, P. Argurio, F. Chidichimo, M. De Biase, S. Straface, E. Curcio, An integrated membrane distillation, photocatalysis and polyelectrolyte-enhanced ultrafiltration process for arsenic remediation at point-of-use, Desalination 520 (2021) 115378, https://doi.org/10.1016/j.desal.2021.115378.
[38] H. Yang, W.-Y. Lin, K. Rajeshwar, Homogeneous and heterogeneous photocatalytic reactions involving AS(III) and as(v) species in aqueous media, J. Photochem. Photobiol. A Chem. 123 (1999) 137–143, https://doi.org/10.1016/S1010-6030(99)00052-0.
[39] A. Figoli, I. Fuoco, C. Apollaro, M. Chabane, R. Mancuso, B. Gabriele, R. De Rosa, G. Vespasiano, D. Barca, A. Criscuoli, Arsenic-contaminated groundwaters remediation by nanofiltration, Sep. Purif. Technol. 238 (2020) 116461, https://doi.org/10.1016/j.seppur.2019.116461.
[40] X.C. Le, S. Yalcin, M. Ma, Speciation of submicrogram per liter levels of arsenic in water: on-site species separation integrated with sample collection, Environ. Sci. Technol. 34 (2000) 2342–2347, https://doi.org/10.1021/es991203u.
[41] S. Santoro, V. Sebastian, A.J. Moro, C.A.M. Portugal, J.C. Lima, I.M. Coelhoso, J. G. Crespo, R. Mallada, Development of fluorescent thermoresponsive nanoparticles for temperature monitoring on membrane surfaces, J. Colloid Interface Sci. 486 (2017) 144–152, https://doi.org/10.1016/j.jcis.2016.09.059.
[42] L. Eykens, K. De Sitter, C. Dotremont, L. Pinoy, B. Van der Bruggen, Membrane synthesis for membrane distillation: a review, Sep. Purif. Technol. 182 (2017) 36–51, https://doi.org/10.1016/j.seppur.2017.03.035.
[43] L. Li, K.K. Sirkar, Influence of microporous membrane properties on the desalination performance in direct contact membrane distillation, J. Memb. Sci. 513 (2016) 280–293, https://doi.org/10.1016/j.memsci.2016.04.015.
[44] M.S. El-Bourawi, Z. Ding, R. Ma, M. Khayet, A framework for better understanding membrane distillation separation process, J. Memb. Sci. 285 (2006) 4–29, https://doi.org/10.1016/j.memsci.2006.08.002.
[45] T. Marino, F. Russo, A. Figoli, The formation of polyvinylidene fluoride membranes with tailored properties via vapour/non-solvent induced phase separation, Membranes (basel). 8 (2018) 71, https://doi.org/10.3390/membranes8030071.
[46] G. Ji, W. Wang, H. Chen, S. Yang, J. Sun, W. Fu, B. Yang, Z. Huang, Sustainable potassium chloride production from concentrated KCl brine via a membrane-promoted crystallization process, Desalination 521 (2022) 115389, https://doi.org/10.1016/j.desal.2021.115389.
[47] S. Simone, A. Figoli, A. Criscuoli, M.C. Carnevale, A. Rosselli, E. Drioli, Preparation of hollow fibre membranes from PVDF/PVP blends and their application in VMD, J. Memb. Sci. 364 (2010) 219–232, https://doi.org/10.1016/j.memsci.2010.08.013.
[48] S. Banerjee, D.D. Dionysiou, S.C. Pillai, Self-cleaning applications of TiO2 by photo-induced hydrophilicity and photocatalysis, Appl. Catal. B Environ. 176–177 (2015) 396–428, https://doi.org/10.1016/j.apcatb.2015.03.058.
[49] Q. Wang, Z. Wang, J. Zhang, J. Wang, Z. Wu, Antifouling behaviours of PVDF/NANO-TiO2 composite membranes revealed by surface energetics and quartz crystal microbalance monitoring, RSC Adv. 4 (2014) 43590–43598, https://doi.org/10.1039/C4RA07274J.
[50] H. Rawindran, J.-W. Lim, P.-S. Goh, M.N. Subramaniam, A.F. Ismail, N.M. Radi bin Nik, M. Daud, M. Rezaei-Dasht Arzhandi, Simultaneous separation and degradation of surfactants laden in produced water using PVDF/TiO2 photocatalytic membrane, J. Clean. Prod. 221 (2019) 490–501, https://doi.org/10.1016/j.jclepro.2019.02.230.
[51] D.-M. Wang, J.-Y. Lai, Recent advances in preparation and morphology control of polymeric membranes formed by nonsolvent induced phase separation, Curr. Opin. Chem. Eng. 2 (2013) 229–237, https://doi.org/10.1016/j.coche.2013.04.003.
[52] C.A. Smolders, A.J. Reuvers, R.M. Boom, I.M. Wienk, Microstructures in phase-inversion membranes. part 1. formation of macrovoids, J. Memb. Sci. 73 (1992) 259–275, https://doi.org/10.1016/0376-7388(92)80134-6.
[53] H. Strathmann, K. Kock, P. Amar, R.W. Baker, The formation mechanism of asymmetric membranes, Desalination 16 (1975) 179–203, https://doi.org/10.1016/S0011-9164(00)82092-5.
[54] M. Drobek, A. Figoli, S. Santoro, N. Navascués, J. Motuzas, S. Simone, C. Algieri, N. Gaeta, L. Querze, A. Trotta, G. Barbieri, R. Mallada, A. Julbe, E. Drioli, PVDF-MFI mixed matrix membranes as VOCs adsorbers, Microporous Mesoporous Mater. 207 (2015) 126–133, https://doi.org/10.1016/j.micromeso.2015.01.005.
[55] E. Drioli, A. Ali, S. Simone, F. Macedonio, S.A. AL-Jlil, F.S. Al Shabonah, H.S. Al-Romaih, O. Al-Harbi, A. Figoli, A. Criscuoli, Novel PVDF hollow fiber membranes for vacuum and direct contact membrane distillation applications, Sep. Purif. Technol. 115 (2013) 27–38, https://doi.org/10.1016/j.seppur.2013.04.040.
[56] R.N. Wenzel, Resistance of solid surfaces to wetting by water, Ind. Eng. Chem. 28 (1936) 988–994, https://doi.org/10.1021/ie50320a024.
[57] S. Santoro, E. Drioli, A. Figoli, Development of novel ECTFE coated PP composite hollow-fiber membranes, Coatings 6 (2016) 40.
[58] E. Guillen-Burrieza, M.O. Mavukkandy, M.R. Bilad, H.A. Arafat, Understanding wetting phenomena in membrane distillation and how operational parameters can affect it, J. Memb. Sci. 515 (2016) 163–174, https://doi.org/10.1016/j.memsci.2016.05.051.
[59] P. Allende, L. Barrientos, A. Orera, M.A. Laguna-Bercero, N. Salazar, M. L. Valenzuela, C. Diaz, TiO2/SiO2 composite for efficient protection of UVA and UVB rays through of a solvent-less synthesis, J. Clust. Sci. 30 (2019) 1511–1517, https://doi.org/10.1007/s10876-019-01594-9.
[60] S. Santoro, I. Vidorreta, I. Coelhoso, J.C. Lima, G. Desiderio, G. Lombardo, E. Drioli, R. Mallada, J. Crespo, A. Criscuoli, A. Figoli, Experimental evaluation of the thermal polarization in direct contact membrane distillation using electrospun nanofiber membranes doped with molecular probes, Molecules 24 (2019) 638.
[61] E. Curcio, E. Drioli, Membrane distillation and related operations—A review, Sep. Purif. Rev. 34 (2005) 35–86, https://doi.org/10.1081/SPM-200054951.
[62] F. Russo, S. Santoro, F. Galiano, C. Ursino, E. Avruscio, E. Di Nicolò, G. Desiderio, G. Lombardo, A. Criscuoli, A. Figoli, A luminescent thermosensitive coating for a non-invasive and in-situ study of thermal polarization in hollow fiber membranes, J. Memb. Sci. 685 (2023) 121928, https://doi.org/10.1016/j.memsci.2023.121928.
[63] M. Rosales, J. Orive, R. Espinoza-González, R. Fernández de Luis, R. Gauvin, N. Brodusch, B. Rodríguez, F. Gracia, A. García, Evaluating the bi-functional capacity for arsenic photo-oxidation and adsorption on anatase TiO2 nanostructures with tunable morphology, Chem. Eng. J. 415 (2021) 128906, https://doi.org/10.1016/j.cej.2021.128906.
[64] N. Barka, S. Qourzal, A. Assabbane, A. Nounah, Y. Ait-Ichou, Photocatalytic degradation of an azo reactive dye, reactive yellow 84, in water using an industrial titanium dioxide coated media, Arab. J. Chem. 3 (2010) 279–283, https://doi.org/10.1016/j.arabjc.2010.06.016.
[65] N. Daneshvar, M. Rabbani, N. Modirshahla, M.A. Behnajady, Kinetic modeling of photocatalytic degradation of acid red 27 in UV/TiO2 process, J. Photochem. Photobiol. A Chem. 168 (2004) 39–45, https://doi.org/10.1016/j.jphotochem.2004.05.011.
[66] Y.-W. Chen, Y.-H. Hsu, Effects of reaction temperature on the photocatalytic activity of TiO2 with pd and cu cocatalysts, Catalysts 11 (2021), https://doi.org/10.3390/catal11080966.
[67] X. Wang, Y. He, Y. Hu, G. Jin, B. Jiang, Y. Huang, Photothermal-conversion-enhanced photocatalytic activity of flower-like CuS superparticles under solar light irradiation, Sol. Energy. 170 (2018) 586–593, https://doi.org/10.1016/j.solener.2018.06.022.
[68] M. Bissen, M.M. Vieillard-Baron, A.J. Schindelin, F.H. Frimmel, TiO2-catalyzed photooxidation of arsenite to arsenate in aqueous samples, Chemosphere 44 (2001) 751–757, https://doi.org/10.1016/S0045-6535(00)00489-6.
[69] A. García, M. Rosales, M. Thomas, G. Golemme, Arsenic photocatalytic oxidation over TiO2-loaded SBA-15, J. Environ. Chem. Eng. 9 (2021) 106443, https://doi.org/10.1016/j.jece.2021.106443.
[70] S. Leong, A. Razmjou, K. Wang, K. Hapgood, X. Zhang, H. Wang, TiO2 based photocatalytic membranes: a review, J. Memb. Sci. 472 (2014) 167–184, https://doi.org/10.1016/j.memsci.2014.08.016.
[71] X. Guan, J. Du, X. Meng, Y. Sun, B. Sun, Q. Hu, Application of titanium dioxide in arsenic removal from water: a review, J. Hazard. Mater. 215–216 (2012) 1–16, https://doi.org/10.1016/j.jhazmat.2012.02.069.
[72] R. Molinari, A.H. Avci, P. Argurio, E. Curcio, S. Meca, M. Plà-Castellana, J. L. Cortina, Selective precipitation of calcium ion from seawater desalination reverse osmosis brine, J. Clean. Prod. 328 (2021) 129645, https://doi.org/10.1016/j.jclepro.2021.129645.
[73] Y. Tang, Y. Lin, W. Ma, X. Wang, A review on microporous polyvinylidene fluoride membranes fabricated via thermally induced phase separation for MF/UF application, J. Memb. Sci. 639 (2021) 119759, https://doi.org/10.1016/j.memsci.2021.119759.

[74] H. Dzinun, M.H.D. Othman, A.F. Ismail, T. Matsuura, M.H. Puteh, M.A. Rahman, J. Jaafar, Stability study of extruded dual layer hollow fibre membranes in a long operation photocatalysis process, Polym. Test. 68 (2018) 53–60, https://doi.org/10.1016/j.polymertesting.2018.03.048.

[75] S. Li, X. Zhao, H. Zhang, Aging retardation strategy of PVDF membranes: evaluation of free radical scavenging effect of nano-particles, New J. Chem. 45 (2021) 6108–6119, https://doi.org/10.1039/D0NJ05980C.

[76] E. Roubaud, W. Maréchal, O. Lorain, L. Lamaa, L. Peruchon, C. Brochier, J. Mendret, J.-P. Mericq, S. Brosillon, C. Faur, C. Causserand, Understanding aging mechanisms in the context of UV irradiation of a low fouling and self-cleaning PVDF-PVP-TiO2 hollow-fiber membrane, Membranes (basel). 12 (2022), https://doi.org/10.3390/membranes12050538.